JOURNAL OF APPLIED ELECTROCHEMISTRY **15** (1985) 807–824

Enhanced mass transfer at the rotating cylinder electrode: III. Pilot and production plant experience

D. R. GABE, F. C. WALSH*

Department of Materials Engineering and Design, The University of Technology, Loughborough, Leicester, LE11 3TU, UK

Received 27 April 1984; revised 17 December 1984

Enhanced mass transfer at a rotating cylinder electrode, due to the development of surface roughness of a metal deposit, has been studied in a range of commercial and pilot scale reactors known as ECO-CELLS. The data obtained for relatively restricted ranges of process parameters show reasonable agreement with the more definitive data obtained under laboratory conditions. With scale-up factors of approximately six times in terms of the rotating cylinder diameter, enhanced mass transfer factors of up to 30 times are reported (in comparison with hydrodynamically smooth electrodes) due to the development of roughened deposits during the process of metal extraction from aqueous solution.

Nomenclature

a, b, c	constants in Equation 15
A	active area of rotating cylinder (cm^2)
C	(bulk) concentration of metal ($mol\,cm^{-3}$ or $mg\,dm^{-3}$)
ΔC	concentration change over reactor ($mol\,cm^{-3}$ or $mg\,dm^{-3}$)
C_{IN}, C_{OUT}, C_{CELL}	inlet, outlet and reactor concentrations of metal ($mol\,cm^{-3}$ or $mg\,dm^{-3}$)
d	diameter of rotating cylinder (cm)
D	diffusion coefficient ($cm^2\,s^{-1}$)
f_R	fractional conversion
F	Faraday constant = 96 500 A s (mol^{-1})
I	current (A)
I_L	limiting current (A)
I_o	useful current (A)
j'_D	mass transport factor ($= St\ Sc^c$)
K	constant in Equation 27
K_L	mass transport coefficient ($cm\,s^{-1}$)
m	slope of Fig. 8 (s^{-1})
M	molar mass of copper = 63.54 g mol^{-1}
n	number of elements in the cascade
N	volumetric flow rate ($cm^3\,s^{-1}$)
p	Reynolds number exponent for powder formation (Equation 28)
R	total cell resistance (Ω)
t	time (s)
U	peripheral velocity of cylinder ($cm\,s^{-1}$)
V_{cell}	cell voltage (V)
V_R, V_T	effective cell, reservoir volume (cm^3)
W	electrolytic power consumption (W)
x	velocity index in Equation 27
z	number of electrons
Re	Reynolds number $= Ud/v$
Sc	Schmidt number $= v/D$
St	Stanton number $= K_L/U$
v	kinematic viscosity ($cm^2\,s^{-1}$)
ϕ	cathode current efficiency
ω	rotational speed (revolutions min^{-1})
ε	peak to valley roughness (cm)

*Present address: Department of Pure and Applied Chemistry, University of Strathclyde, 295 Cathedral Street, Glasgow G1 1XL, UK.

0021–891X/85 $03.00 + .12

1. Introduction

In Parts I and II [1, 2] a laboratory investigation of a rotating cylinder electrode reactor was described in which electrodeposition of metal normally took place at limiting current densities, under complete mass transfer control. The development of powder or dendritic growth enabled enhanced mass transfer to be achieved by virtue of the combination of increased hydrodynamic shear and increased electroactive area. Reactors of this type were developed by Holland [3–5] for the ECO-CELL process whose particular virtue was originally considered to be the enhanced mass transfer which occurred: other virtues are now appreciated including the possibility of full potentiostatic control which enables cathodic separation of metals to be attained [4, 6, 7].

Two families of ECO-CELL reactor have been developed. Firstly, the simple rotating cylinder geometry has been scaled-up over almost two orders of magnitude – duty being expressed simply in terms of current carrying capacity (see Table 1 for other details). Secondly, the cascade cell configuration (which has been described fully elsewhere [4, 8]) has been used primarily as a 'polishing' cell to remove last traces of metal from liquors and effluents. Experimental work undertaken on each model was aimed at evaluating performance and investigating the parameters for reactor scale-up. The main reaction used was the deposition of copper from 0.5 M sulphuric acid. Cathode polarization characteristics were measured and performance was indexed by an analysis of the mass transport and conversion in the reactor. Several modes of operation were considered, including single pass, batch recycle and cascade configurations.

2. Reaction design

2.1. *Rotating cylinder electrode reactor (RCER)*

It is obvious that in a development programme many changes take place in a reactor design and no precise uniformity should be expected. The design theory has been discussed elsewhere [9] and so a detailed description of one model only will be given here. The main dimensions of the 500 A model are given in Table 1 and the schematic plan in Fig. 1. The design essentially incorporates a concentric rotating cylinder, diaphragm, anode and cell, although complete concentricity has to be disturbed to provide fluid manifolds and a scraping mechanism along the length of the cylinder. The main reactor body was fabricated from machined sections of high density polypropylene joined together by welding and with flanges at the top and bottom to facilitate mounting and dismantling. (Other constructional materials included titanium and rubber-coated mild steel.) The reactor body was secured via its top flange to a horizontal, coated steel platform which also supported a mechanical packed gland, shaft seal assembly which was lubricated with water. The 7.5 cm diameter stainless steel drive shaft was supported by two vertical roller bearing races and was driven by a 4 kW d.c. motor coupled through a 1:1 pulley and belt system allowing rotational speeds of 100 to 1000 r.p.m. Faradaic power was supplied

Table 1. Characteristics of ECO-CELL assemblies available for mass transfer studies

Reactor model	*Nominal current capacity (A)*	*Cylinder diameter d(cm)*	*No. of compartments, n*	*Electrode area, A (cm^2)*	*Rotational speed, ω(r.p.m.)*	*Peripheral velocity, U ($cm\,s^{-1}$)*
Laboratory rig	50	7.62	(1)	200	600–3000	239–1200
Mini-cell	100	10.2	(1)	200	500–1500	266–797
Small pilot plant	500	23.5	(1)	1633	100–1380	123–1698
Mobile rig	500	24.8	(1)	1980	239–760	975
Large pilot plant	2000	45.1	(1)	5757	460	1086–1112
Laboratory cascade	100	7.6	10	10 × 215	2000	796
Pilot plant cascade	200	30.6	6	6 × 1387	730	1170
Commercial cascade	1000	32.4	12	12 × 2036	860	1459

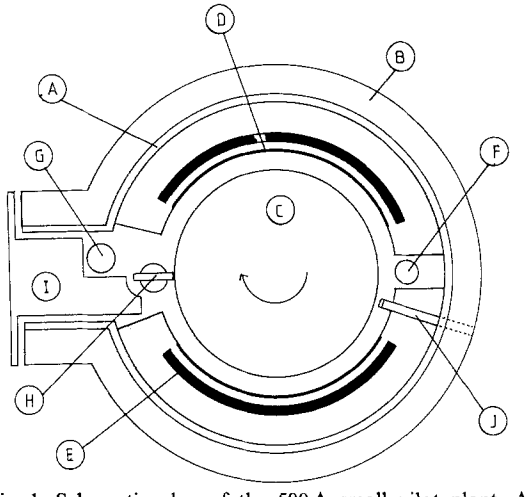

Fig. 1. Schematic plan of the 500 A small pilot plant. A reactor body, B top flange, C rotating cylinder electrode, D cationic exchange membrane, E anodes (2), F inlet sparge tube, G outlet tube, H scraper, I polypropylene insert and J reference electrode probe.

to the shaft by eight spring loaded graphite brushes and a small auxiliary brush located near the cylinder acted as a potential pick-up.

The rotating cylinder consisted of a hollow mild steel fabrication, copper-plated on its working surface and with polypropylene end caps giving electroactive dimensions of diameter 22.9 cm, length 22.7 cm and total area 1633 cm^2. The cylinder was fitted to the shaft by heat shrinking. Several scraper devices were feasible [10] but the one favoured in this model was a stellite-tipped blade located on a vertical shaft driven pneumatically in a vertical plane: thus it could be used intermittently to traverse the length of the cylinder, in a reciprocating fashion.

The bottom cover of the reactor carried inlet and outlet manifold tubes of 12.5 mm inside diameter polypropylene running parallel to the axis of the cylinder. The inlet tube had 16 holes (5 mm each) promoting good fluid dispersion while the outlet had 40 holes (10 mm each) thereby preventing blockage by product metal powders and consequent pressurizing of the compartment. The anolyte and catholyte compartments were separated by a perfluorocarbon cation exchange membrane, Nafion type 425 (DuPont, Wilmington Delaware), supported by a perforated polypropylene screen. Precious metal oxide/titanium anodes of the 'DSA' type (supplied by Diamond Shamrock) were used.

The electrolyte flow system is shown schematically in Fig. 2. The catholyte was stored and mixed in a temperature-controlled polypropylene

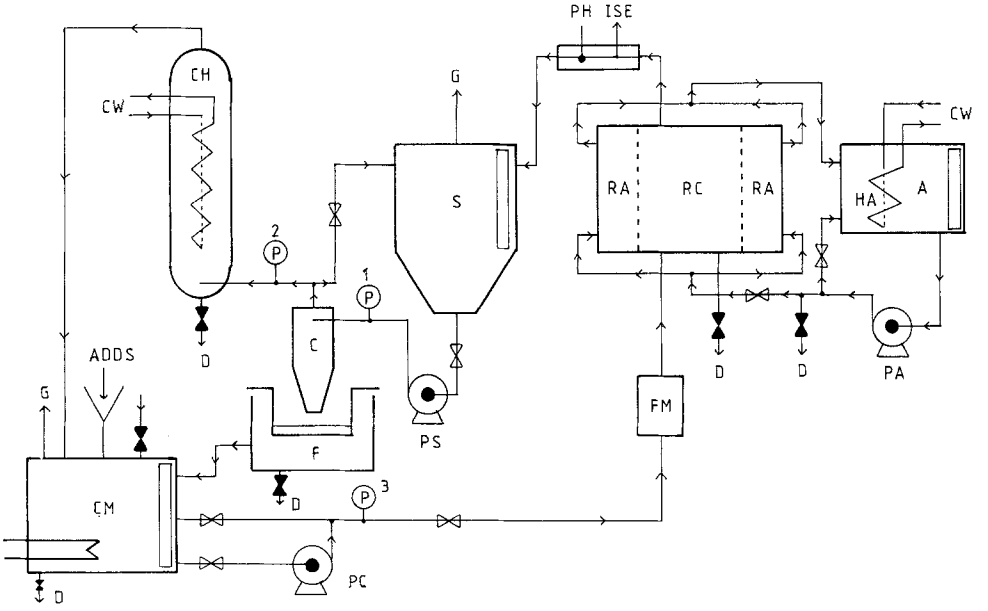

Fig. 2. Schematic flow diagram for the 500 A small pilot plant. RC catholyte compartment, RA anolyte compartment, CH catholyte heat exchanger, HA anolyte heat exchanger, FM flow meter, S gas–liquid separator, C hydrocyclone solid–liquid separator, F filter tank and tray, CM catholyte mixing tank, PC catholyte pump, PA anolyte pump, PS separator pump, PH pH/reference electrodes, ISE ion selective electrode sampling bleed, ADDS chemical additions, A anolyte, CW cooling water, G gas vent and D to drain.

tank provided with a gas vent and dosing inlet. No attempt was made to deoxygenate the solution as this was not considered practical nor standard industrial practice. Solution was pumped to the reactor through a magnetic flux flow meter with bypass loop flow control, and was limited to a total effective volume of 400 dm^3. After passage through the reactor the catholyte was vented in a conical gas separator and metal powder was removed as a slurry in a hydrocyclone solid–liquid separator. The powder was subsequently filtered and the catholyte flow balanced for storage or recycling. The anolyte, 0.5 M H_2SO_4, was continuously circulated at 40° C and 5 $dm^3 min^{-1}$, the total inventory being 30 dm^3. Solutions were analysed by discrete sampling followed by atomic absorption spectrophotometry, or continuous ion selective electrode monitoring [11].

Faradaic d.c. power was supplied from a Westinghouse transformer/rectifier set of capacity 500 A/12 V through aluminim busbars and copper cored flexible leads. Electrode potentials were monitored with a $Hg/Hg_2SO_4/1$ M Na_2SO_4 reference electrode using a polypropylene tube and ceramic frit probe positioned 4 mm from the cylinder. While a smaller gap would have reduced IR drop the 4 mm was considered necessary in order to allow build-up of metal powder.

Table 2. Essential characteristics relating to the 500 A small pilot plant reactor trials

Rotating cylinder cathode	
Material	copper-plated steel
Diameter, d	22.9 cm
Effective length, l	22.7 cm
Effective area, A	1633 cm^2
Rotational speed, ω	500 revs min^{-1}
Peripheral velocity, U	600 cm s^{-1}
Catholyte	0.5 M H_2SO_4 + Cu (34 to 560 mg dm^{-3})
Nominal catholyte temperature	60° C
Effective catholyte volume, V_T	406 dm^3
Nominal catholyte flow rate, N	40 $dm^3 min^{-1}$
Kinematic viscosity, ν	5.91 × 10^{-3} $cm^2 s^{-1}$
Diffusion coefficient, D	1.24 × 10^{-5} $cm^2 s^{-1}$
Schmidt number, Sc	477
Reynolds number, Re	2.32 × 10^6

Polarization curves were obtained by manually increasing the cathode potential, typically in 25 mV increments; steady currents were then measured. Reactor performance was investigated by measuring the current and monitoring the concentration histories of dissolved copper in the catholyte. All temperatures, flow rates and rotation speeds were controlled and measured.

The nominal conditions employed in the 500 A small pilot plant trials are summarized in Table 2.

2.2. *Cascade cell*

The specifications of three cascade cells are given in Table 1. The 100 A and 1000 A models represented an early horizontal design concept which was superceded by the 200 A vertical model which included a scraper, removable baffles for the catholyte compartments and removable membrane. A schematic plan is shown in Fig. 3. The reactor body was of rubber-coated mild steel with regularly spaced polypropylene baffle plates giving a nominal gap of 3 mm. The

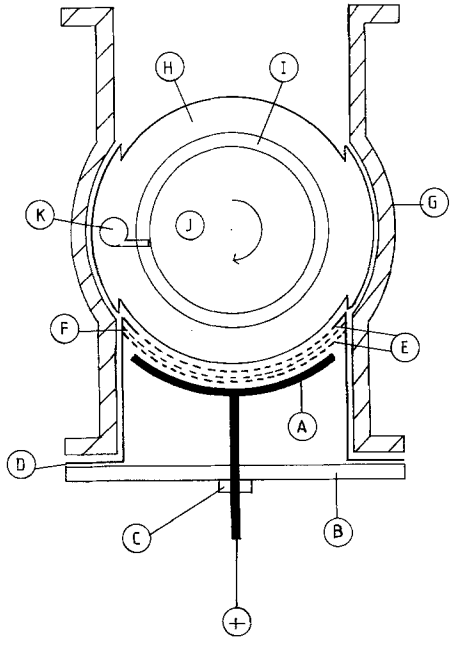

Fig. 3. Schematic plan of the 200 A cascade cell reactor. A anode, B anode box securing plate, C insulating bush, D titanium plate anode compartment, E perforated titanium membrane supports, F cationic exchange membrane, G catholyte reactor body, H catholyte dividing baffle plate, I baffle-cylinder space (annular), J rotating cylinder electrode and K scraper.

cathode cylinder (diameter 30.6 cm) of stainless steel with polypropylene end caps, was supported by top and bottom bearings sealed at each end, and was driven at 730 r.p.m. by an a.c. motor, substantially oversized at a rated 13 kW. Two anolyte compartments were inserted into the reactor sides and a Nafion cation exchange membrane, type 425 was supported by two perforated titanium plates. The anode compartments were each equipped with three separate curved nickel anodes. Each of the six catholyte compartments, of length 14.4 cm, was equipped with a sample point and reference electrode probe.

The total flow system is shown schematically in Fig. 4. The anolyte solution was 2.5 M NaOH stored in a 200 dm^3 tank with a gas venting facility. NaOH was preferred to H_2SO_4 for the cascade reactor as the former allowed the use of nickel anodes rather than the precious metal based type normally necessary in acidic conditions. Anolyte was circulated at 30° C and 25 $dm^3 min^{-1}$. The catholyte, consisting of 0.5 M H_2SO_4 containing up to 1000 ppm copper, was maintained at constant temperature in a rubber-lined steel tank of 3000 dm^3 capacity. It was pumped upwards through the cascade reactor and afterwards treated for gas and solids separation.

The electrical connections are shown in Fig. 5 and can be divided into electrolytic current supply and potential monitoring circuits. Electrolytic d.c. power capacity was 500 A/16 V, although the working capacity was limited to 300 A which was applied to the cathode through copper-filled graphite brushes working against a copper slip ring. Anode connections were arranged to engage any number of the three pairs of anodes. Rotational power was provided by a three-phase a.c. motor at 730 r.p.m. Cathode potentials were monitored in each compartment using a polypropylene/ceramic frit probe; cylinder potentials were sensed by potential pick-up brushes located on the top and bottom shafts of the cylinder.

Three types of experiment were carried out. Cathode polarization data were generated by increasing the total cell current in increments and monitoring individual compartment potentials. Steady state electrolysis was carried out at a set temperature, flow rate and cell current; instantaneous inlet and outlet copper levels were monitored. In batch decay experiments, the copper level was allowed to fall when reservoir dosing ceased; the decline in cell current, inlet and outlet copper levels was monitored.

3. Results

Mass transport data were calculated from the results of experiments involving polarization curves and electrolysis in the presence and absence of a copper concentrate dosed into the reservoir. Because the prime purpose of an ECO-CELL reactor is normally to strip metal

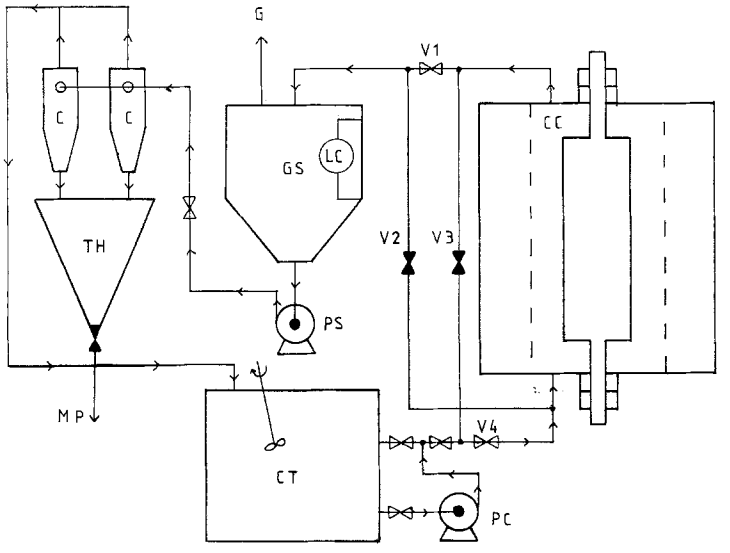

Fig. 4. Schematic flow diagram for the 200 A cascade cell reactor. CC catholyte compartment, PC catholyte pump, GS gas–liquid separator, G gas vent, C hydrocyclone solid–liquid separator, TH thickening cone, MP metal powder slurry, CT catholyte tank, PS separator pump and LC level control for GS. For metal removal: V1, V4 open; V2, V3 closed. For metal backwash: V1, V4 closed, V2, V3 open.

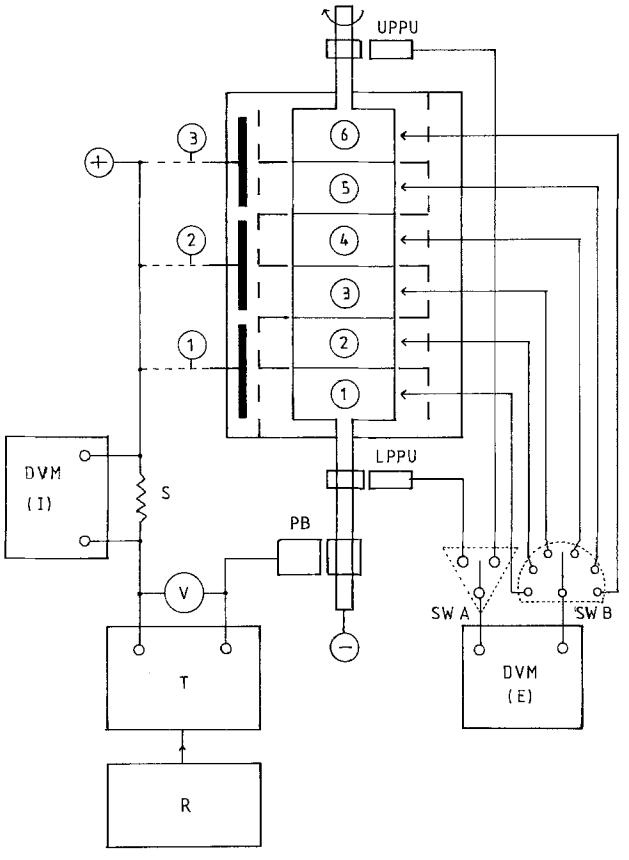

Fig. 5. Schematic electrical circuit for the 200 A cascade cell reactor. T transformer/rectifier, R regulator, S precision shunt (500 A/50 mV), V cell voltmeter, LPPU lower potential pick-up brush, UPPU upper potential pick-up brush, DVM(I) current meter, DVM(E) potential meter and SWB switch to reference electrodes. (RHS anodes omitted for clarity).

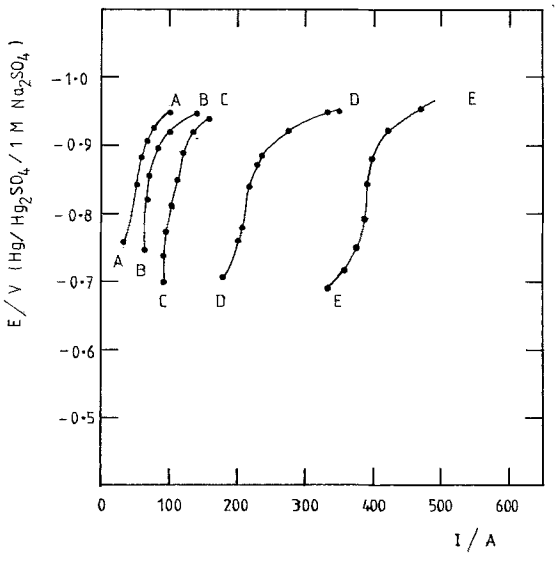

Fig. 6. (500 A) small pilot plant reactor. Polarization curves in the vicinity of the limiting current. Exit copper concentrations: A: 40; B: 59; C: 95; D: 175; E: 292 mg dm^{-3}.

from solution it is very difficult to obtain meaningful polarization curves in a high duty, flow through reactor. The metal concentration is continually falling as the current is raised due to the increasing conversion in the reactor. Thus manually obtained potentiodynamic-type curves do not exhibit truly constant limiting current densities; however, by measuring the current over a restricted range of potential, near the limiting current, for example -950 to -700 mV versus $Hg/Hg_2SO_4/1\ M\ Na_2SO_4$, and relating the data to instantaneous concentration values, a pseudo steady state mass transfer analysis can be achieved. Such polarization curves (Fig. 6) can directly provide mass transfer data, as in Table 3 which gives a linear limiting current–concentration relationship (not shown) whose slope gives an average value of $K_L = 0.270$ cm s^{-1}.

The polarization curves provided a guide to potentials corresponding to the limiting current

Table 3. Mass transport coefficients for copper in the 500A small pilot plant reactor

Limiting current $I_L(A)$	*Limiting current density* $i_L(A\,cm^{-2})$	*Reactor concentration,* C_{cell}		*Mass transport coefficient* $K_L(cm\,s^{-1})$
		$(mg\,dm^{-3})$	$(\mu mol\,cm^{-3})$	
484	0.296	360	5.67	0.271
385	0.236	292	4.60	0.266
218*	0.133	175	2.75	0.251
175	0.107	138	2.17	0.256
112*	0.069	95	1.50	0.238
72*	0.044	59	0.93	0.246
54*	0.033	40	0.63	0.272

*From the polarization curves of Fig. 6.

plateau regions where copper deposition was under mass transport control.

A series of electrolysis trials was carried out potentiostatically under steady state conditions (as in Table 2) at potentials in the range -800 to -950 mV versus $Hg/Hg_2SO_4/1\ M\ Na_2SO_4$. The reservoir was normally continuously dosed with a copper concentrate to maintain a reasonable inlet copper concentration to the reactor. Selected results are shown in Table 4. The reactor may be treated as a single pass, continuously stirred tank reactor (CSTR) under mass transport control [9, 12] and mass transport data were abstracted from conversion data as follows.

According to Faraday's laws, the current associated with copper deposition (and hence removal) is given by:

$$\Delta C = C_{IN} - C_{OUT} = \frac{I_{Cu}}{2FN} \quad (1)$$

$$I_{Cu} = 2FN\Delta C \quad (2)$$

where I_{Cu} has units of amps if N is expressed in $cm^3\,s^{-1}$ and ΔC in $mol\,cm^{-3}$. If the more convenient units of mg dm^{-3} are used for C,

$$I_{Cu} = \frac{2FN\Delta C}{M\,10^3} = \frac{N\Delta C}{0.329} \quad (3)$$

Assuming the copper deposition reaction to be under complete mass transport control, $I_{Cu} = I_L$ and the mass transport coefficient may be calulated using the definition:

$$K_L = \frac{I_L}{AzFC_{cell}} \quad (4)$$

As a conseqence of CSTR behaviour, $C_{cell} = C_{OUT}$ and Equations 1 and 4 may be combined to enable the conversion to be expressed as

$$\frac{C_{IN}}{C_{OUT}} = 1 + \frac{K_L A}{N} \quad (5)$$

which allows K_L to be calculated directly from conversion data as:

$$K_L = \frac{N}{A}\left(\frac{C_{IN}}{C_{OUT}} - 1\right) \quad (6)$$

Fractional conversion over the reactor may be calculated as

$$f_R = 1 - \frac{C_{OUT}}{C_{IN}} \quad (7)$$

Cathode current efficiency for copper deposition was calculated (as a percentage) via the equation

$$\phi = (I_{Cu}/I)\,100 \quad (8)$$

Table 4 shows individual I_L, K_L, f_R and ϕ values calculated for each trial according to Equations 3, 6, 7 and 8 respectively. The following ranges of each parameter were experienced: $24\,A < I_L < 573\,A$; $0.22\,cm\,s^{-1} < K_L < 0.413\,cm\,s^{-1}$; $0.35 < f_R < 0.51$ and $26\% < \phi < 112\%$. Under complete mass transport control, Equation 4 predicts a linear relationship between I_L and C_{OUT}. Fig. 7 shows such a composite plot of the experimental data; results are shown for the cases of zero and positive reservoir dosing. A least square regression of I_L upon C_{OUT} provided a line from which an overall K_L value could be calculated. The data points have been treated in two ways, firstly as a complete set

Table 4. Selected results for the (500A) small pilot plant reactor

Cathode potential (V) (versus Hg/Hg_2SO_4/ 1 M Na_2SO_4)	*Catholyte temperature (° C)*	V_{cell}	$I(A)$	N ($dm^3\,s^{-1}$)	C_{IN} ($mg\,dm^{-3}$)	C_{OUT} ($mg\,dm^{-3}$)	ΔC ($mg\,dm^{-3}$)	C_{IN}/C_{OUT}	I_{CU} (A)	$\phi(\%)$	K_L ($cm\,s^{-1}$)	f_R
−0.800	60	8.0	448	0.65	500	260	240	1.92	474	106	0.367	0.48
−0.850	60	8.1	500	0.65	560	290	270	1.93	533	107	0.370	0.48
−0.850	60	8.1	450	0.65	490	255	235	1.92	464	103	0.367	0.48
−0.850	60	8.0	500	0.65	550	270	280	2.04	553	110	0.413	0.51
−0.850	60	8.2	500	0.65	550	275	275	2.00	543	109	0.398	0.50
−0.850	60	8.2	510	0.65	585	295	290	1.98	573	112	0.392	0.50
−0.850	57	8.3	510	0.65	525	265	260	1.98	514	101	0.391	0.50
−0.900	60	7.7	415	0.65	380	200	180	1.90	356	86	0.359	0.47
−0.900	60	7.1	372	0.65	360	180	180	2.00	356	96	0.399	0.50
−0.950	58	6.7	359	0.60	267	138	129	1.93	235	65	0.343	0.48
−0.950	58	4.3	182	0.60	195	107	88	1.82	160	88	0.301	0.45
−0.950	58	4.0	160	0.57	130	68	62	1.91	107	67	0.317	0.48
−0.950	58	3.8	142	0.65	71	42	29	1.69	57	40	0.274	0.41
−0.950	58	3.5	112	0.65	48	30	18	1.60	36	32	0.242	0.38
−0.950	58	3.1	91	0.65	34	22	12	1.55	24	26	0.220	0.35

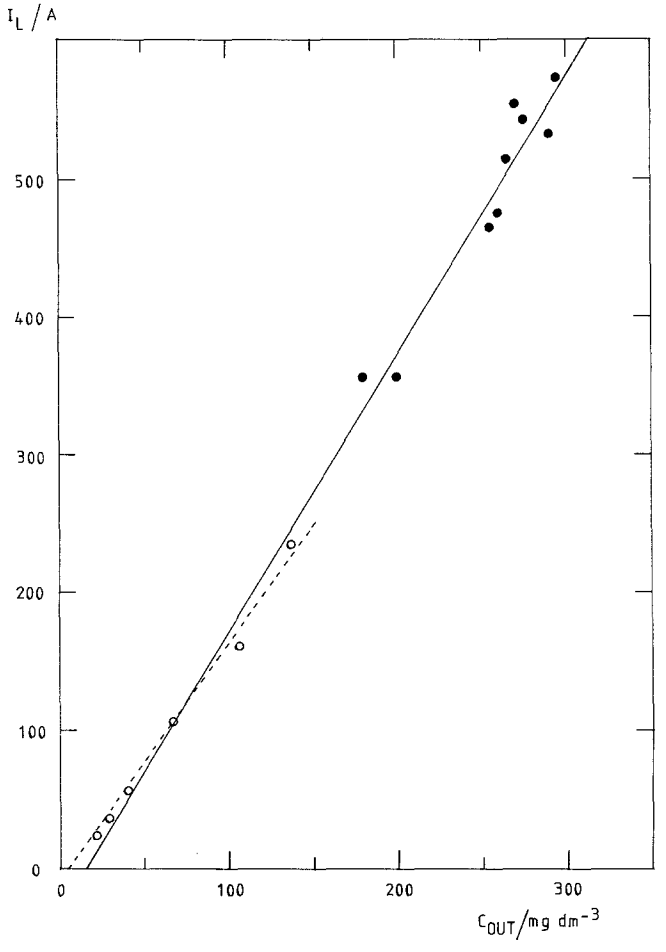

Fig. 7. (500 A) small pilot plant reactor. Calculated limiting current as a function of outlet copper concentration. Conditions as in Table 2. ○ without reservoir dosing (concentration decay), ● with reservoir dosing. The solid line (through all data) gives $K_L = 0.40\,\text{cm s}^{-1}$, the broken line (through concentration decay data) gives $K_L = 0.34\,\text{cm s}^{-1}$. The majority of the data was obtained at $I_L \simeq 500\,\text{A}$ $C_{OUT} \simeq 260\,\text{mg dm}^{-3}$ since this represented the principle operating zone for the reactor.

giving $K_L = 0.40\,\text{cm s}^{-1}$ corresponding to $f_R = 0.49$ and secondly the results for 'zero reservoir dosing' have been treated separately, giving $K_L = 0.34\,\text{cm s}^{-1}$ (corresponding to $f_R = 0.45$). Thus the mass transport coefficient calculated in this manner appeared to show a lower value at reduced copper levels.

In the case of data obtained during the absence of reservoir dosing, the system may be treated as a CSTR reactor in the batch recirculation mode. Under mass transport control, the resultant concentration decay at the reactor inlet may be adequately approximated by [13]

$$C_{IN,t} = C_{IN,o} \exp\left[-\frac{Nt}{V_T}\left(1 - \frac{1}{1 + K_L A/N}\right)\right] \quad (9)$$

which is valid for $V_R \ll V_T$; in practice the values were such that $2\,\text{dm}^3 \ll 406\,\text{dm}^3$. Taking logarithms;

$$\ln C_{IN,t} = \ln C_{IN,o} - \left[\frac{Nt}{V_T}\left(1 - \frac{1}{1 + K_L A/N}\right)\right] \quad (10)$$

Equation 10 predicts that a plot of $\ln C_{IN,t}$ against t should be linear and of slope, m given by:

$$m = -\frac{N}{V_T}\left(1 - \frac{1}{K_L A/N}\right) \quad (11)$$

Fig. 8 shows such a plot, displaying data for both the inlet and outlet concentrations; ideally the slopes should be identical (as required by Equation 5) and given by Equation 11. The overall value of the mass transport coefficient may then be obtained from:

$$K_L = \frac{N}{A}\left(\frac{1}{1 + mV_T/N} - 1\right) \quad (12)$$

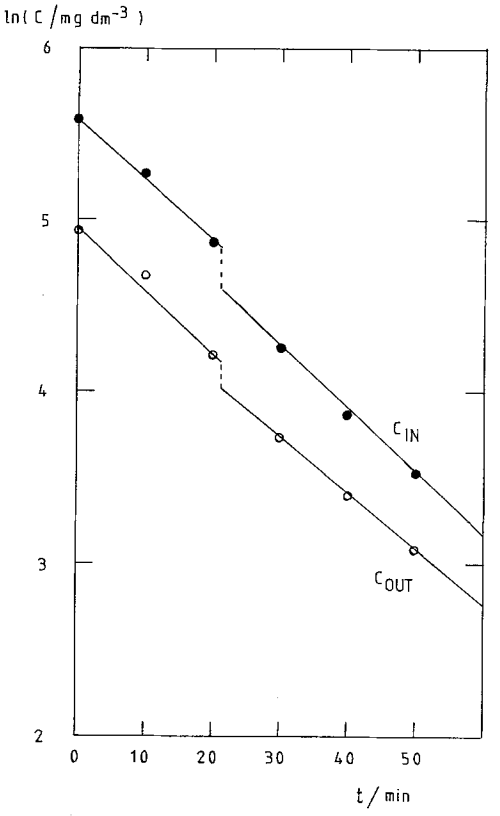

Fig. 8. (500 A) small pilot plant reactor. Logarithm of the copper concentration versus time, showing the inlet (●) and outlet (○) values. Conditions as in Table 2. The line drawn through C_{IN} data gives $K_L = 0.24\,cm\,s^{-1}$. (Note: the break in the lines, at $t = 21$ min, is due to an abrupt fluctuation in the flow conditions.)

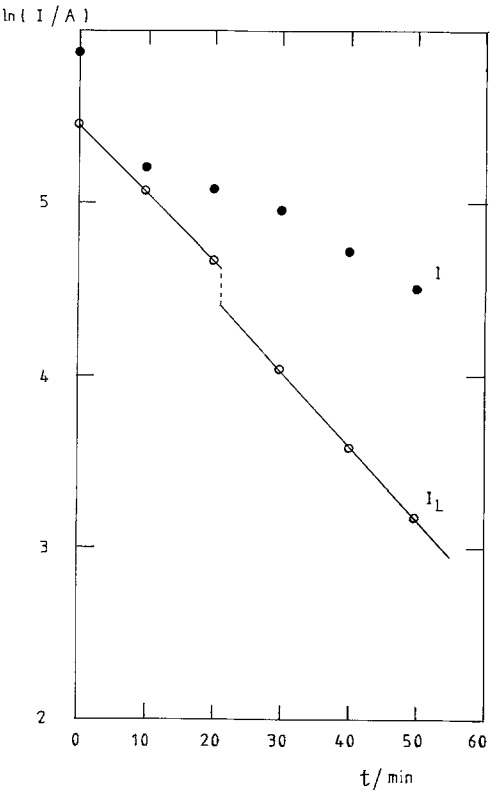

Fig. 9. (500 A) small pilot plant reactor. Logarithm of current versus time: ● cell current; ● calculated limiting current (corresponds to Fig. 8).

where values of N, A and V_T are given in Table 2. A least squares regression of the data yields $K_L = 0.24\,cm\,s^{-1}$ (corresponding to $f_R = 0.37$). The break in the decay curves in Fig. 8 was due to an abrupt change in the flow conditions through the reactor due to operational problems; at $t = 21$ min, the flow rate was rapidly reduced, then it was allowed to stabilize.

Fig. 9 shows the current–time history corresponding to Fig. 8; both the total cell current, I and calculated limiting current, I_L are included. Ideally, I_L should decay in an analogous fashion to C_{IN} or C_{OUT} (as required by Equations 1 and 4:

$$\ln I_{L,t} = \ln I_{L,o}\left[-\frac{Nt}{V_T}\left(1 - \frac{1}{1 + K_L A/N}\right)\right] \quad (13)$$

Fig. 9 indicates a break in the curve corresponding to I_L, for the same reasons as that evident in Fig. 8. It is also evident that the data describing total cell current diverge from the I_L line as time increases, i.e. the current efficiency for copper removal decreased as copper concentration declined. This is attributable to the increasing influence of the secondary reactions (primarily hydrogen evolution but also oxygen reduction) at lower copper levels.

As discussed in detail elsewhere [1, 2, 7], the rate of decay of concentration (and hence the mass transport) is enhanced in comparison to a smooth or machined-rough cathode due to the development of a high surface area and high hydrodynamic shear at the deposit.

Changing the speed of the linearly reciprocating scraping blade in the available range 0.9 to $9.0\,cm\,s^{-1}$ had no apparent effect on f_R (and hence K_L), indicating that, within this range, the mass transport was not a sensitive function of scraping rate.

One further feature is noteworthy. The cell

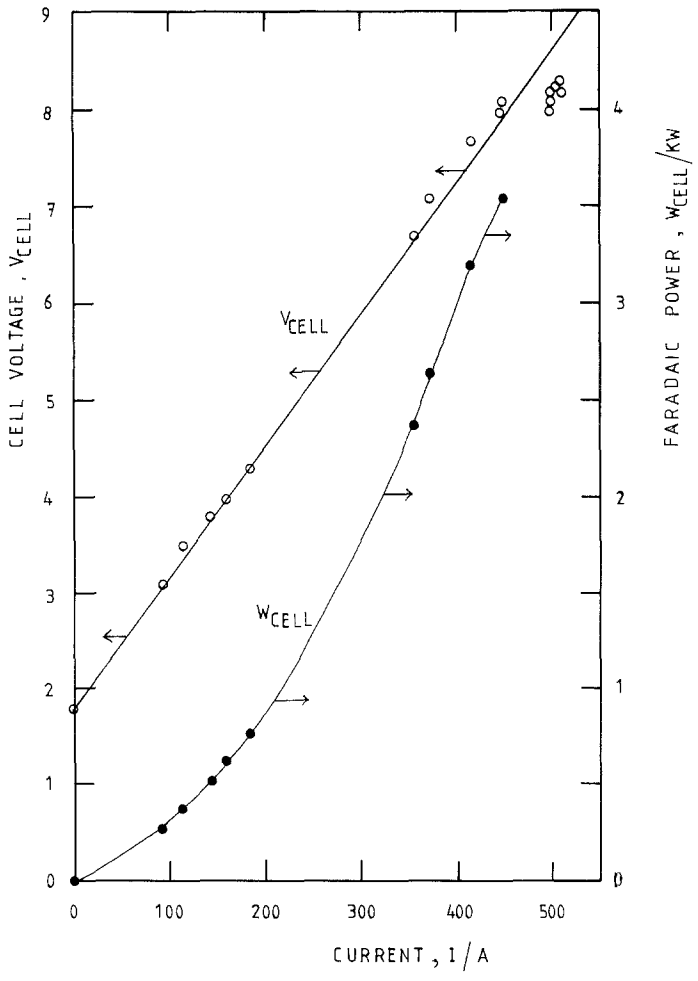

Fig. 10. (500 A) small pilot plant reactor. Cell voltage and electrolytic power consumption as a function of current.

resistance can be deduced from a plot of total cell voltage against total cell current (Fig. 10). The average effective cell resistance was only 0.0138 Ω due to the use of a conductive supporting electrolyte (0.5 M H_2SO_4) and a relatively small cell gap ($\simeq$ 13 mm). The power requirement for electrolysis is also displayed as a function of current and as expected from the relationship: $W = I^2R$, the power increased steeply as the cell current was raised.

The concept of a Cascade ECO-CELL reactor has been previously documented [3, 4] and design considerations have been discussed, together with typical data, in a recent publication [8].

The nominal, predicted performance of this type of cell may be described by means of various simplified design curves, as follows.

Equation 3 representing copper deposition at 100% current efficiency may be rewritten:

$$\Delta C = \frac{0.329 I_L}{N} \tag{14}$$

which expresses the concentration change across the reactor in mg dm^{-3}. As shown in Fig. 11, Equation 14 predicts a series of lines each of slope $0.329/N$ if ΔC is plotted as a function of I_L. This figure shows ranges of experimental data for the 200 A pilot plant cascade reactor. The practical performance was such that overall conversions were lower than the predicted values. This feature, which was particularly noticeable at high currents or lower flow rates is attributable to several factors including

(a) $\phi < 100\%$ due to hydrogen evolution as a secondary reaction, together with a degree of redissolution of copper and

(b) a tendency to bypassing, i.e. internal

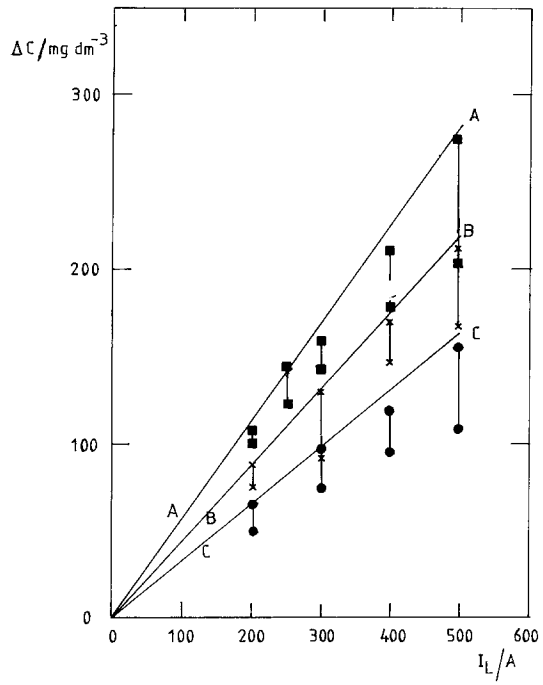

Fig. 11. Idealized concentration difference as a function of current for the 200 A cascade cell reactor at various flow rates. Solid lines: theoretical perfomance for copper deposition at 100% current efficiency (according to Equation 14). Data points: copper removal at 60° C from approximately 0.5 M H_2SO_4, showing the experimental variation. A; $N = 35\,dm^3min^{-1}$ B; $N = 45\,dm^3min^{-1}$ and C; $N = 60\,dm^3min^{-1}$.

channeling of electrolyte from a high concentration to a (non-adjacent) low concentration compartment [8]).

In Parts I and II [1, 2], it was indicated that an equation of the form:

$$j'_D = St\,Sc^c = a\,Re^b \qquad (15)$$

may be used to describe mass transport to a rotating cylinder. If the empirical values of $a = 0.0791$; $b = -0.08$ and $c = -0.644$ due to Holland [4] are assumed, the correlation becomes:

$$St = 0.0791\,Re^{-0.08}\,Sc^{-0.644} \qquad (16)$$

which may be rewritten in terms of the mass transport coefficient,

$$K_L = 0.0791\,Sc^{-0.644}\left(\frac{d}{\nu}\right)^{-0.08} U^{0.92} \qquad (17)$$

For the case of a fixed electrolyte at a constant temperature, Sc is approximately constant (ν and D are primarily dependent upon the H_2SO_4 background electrolyte; the $CuSO_4$ is present at relatively low levels and in a restricted range). Equation 17 may then be simplified to

$$K_L = (constant)\,U^{0.92}\,d^{-0.08} \qquad (18)$$

and a plot of K_L versus $(U^{0.92}d^{-0.08})$ should be linear. An attempt is made to produce such a plot in Fig. 12 which includes experimental data ranges for each of the cascade reactors listed in Table 1. The data refer to the common condition of a 0.5 M H_2SO_4 background electrolyte at 60° C. In order to calculate K_L values for Fig. 12, the following procedure has been used. The analogue of Equation 5 for a cascade reactor consisting of n CSTRs in hydraulic series all operating under mass transport control is

$$\frac{C_{IN}}{C_{OUT,n}} = \left(1 + \frac{K_L A}{N}\right)^n \qquad (19)$$

Taking logarithms,

$$\ln\frac{C_{IN}}{C_{OUT,n}} = n\ln\left(1 + \frac{K_L A}{N}\right) \qquad (20)$$

Equation 20 predicts that a plot of the 'left hand side' against n should be a straight line of slope $\ln(1 + K_L A/N)$. A and N are experimentally fixed and controlled variables and therefore K_L may be calculated. Fig. 13 shows a range of experimental data plotted in comparison to the line predicted by Equation 18. The data, representing the practical performance of three different models [8] of reactor fall below the line, indicating a somewhat lower performance than expected. This is largely attributable to the fact that the K_L (ordinate) values have been calculated as overall ones over a wide range of copper concentrations. As is evident from Fig. 13, a tendency to lower conversion in low concentration (large n) compartments results in data falling below the predicted line. The variation in the experimental mass transport coefficient for a given cascade cell may be attributed to a lower active electrode area and a smaller degree of roughness in low concentration (large n) compartments, together with a decreasing current efficiency (for reasons mentioned above). As shown in Fig. 11, Equation 4 predicts a series of lines of slope $0.329/N$ if ΔC is plotted aginst I.

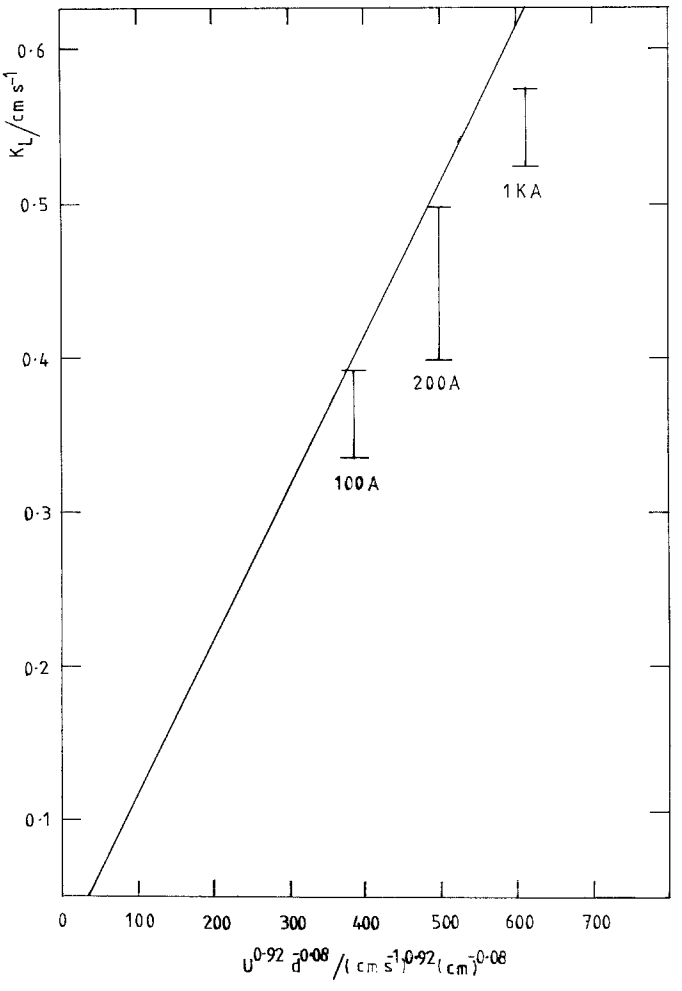

Fig. 12 Mass transport coefficient as a function of $(U^{0.92}d^{-0.08})$ for three cascade reactors. The predicted line is calculated according to Equation 17.

The data points show that, particularly at higher currents or lower flow rates, the actual performance gave conversions somewhat lower than the theoretical values.

The overall resistance of a typical cascade reactor is illustrated as a plot of cell voltage against current in Fig. 14, for the 200 A reactor. The slope of the approximately linear plot is 0.015 Ω, the normal cell voltage being 3.7 V at 299 A.

4. Discussion

Before discussing the detailed behaviour of the various reactors some general comments can be made about their practical performance. The rotating cylinders were readily scraped during a backwash/removal cycle and the powder entrained in the electrolyte flow without difficulty. Once scraped, the smoother cylinder revolved more freely with less vibration and required less rotational power; however, if a point scraper is used a more constant rotational power can be ensured.

If power is scraped off in large quantities intermittently, typically after several hours deposition, the glut can rapidly block the hydrocyclone separation system and other filtration systems might be advantageous. However, 'point-scraping' levels out the separation problem and is therefore preferred [10].

The overall power consumption of the 200 A cascade reactor was approximately 11.5 kW h kg^{-1} for copper, for an inlet copper level of 80 to 120 mg dm^{-3} of which the measured electrolytic and rotational power contributions were 4.9 and

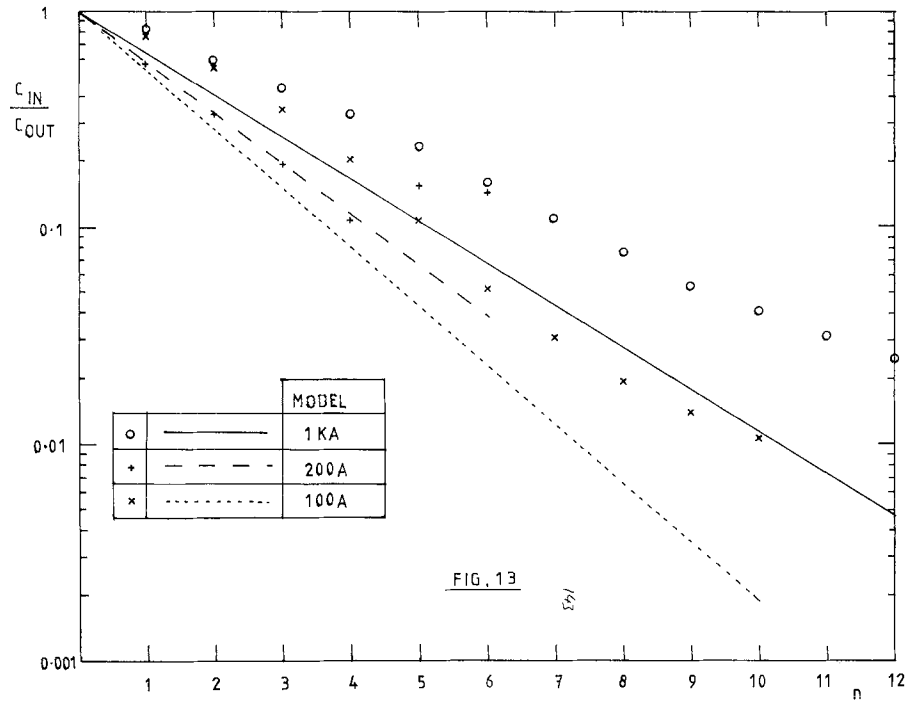

Fig. 13. Concentration ratio: C_{IN}/C_{OUT} as a function of compartment number for three cascade reactors.

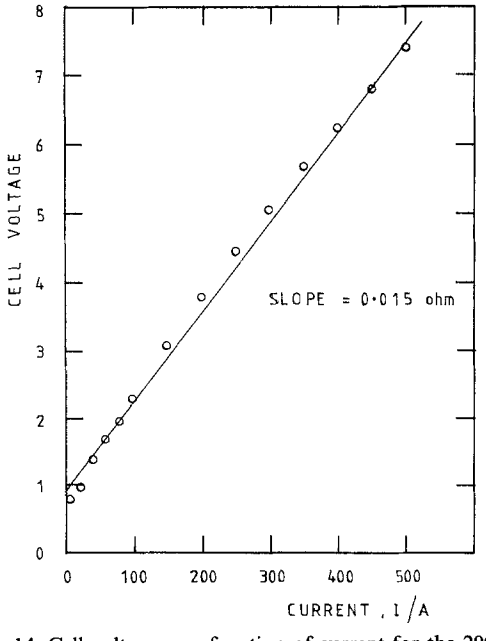

Fig. 14. Cell voltage as a function of current for the 200 A cascade cell. (Hydrogen evolution reaction using anode pair No. 1 only, i.e. the lowest set of anodes in Fig. 5.)

6.6 kW h kg^{-1} respectively. This disproportionate distribution from the rotational component is inevitable when such low concentrations of metal are being treated, together with the high conversion over a single reactor.

By using the pilot plant reactors under specially controlled conditions, it has been possible to obtain sufficient data to make an attempt to perform a mass transfer correlation. For the five RCER cells, for which details are given in Table 1, the data has been plotted as j'_D against Re, where [12]

$$j'_D = St\,Sc^{0.644} = a\,Re^b \qquad (21)$$

and comparison made with Equation 16 which may be rewritten

$$j'_D = 0.0791\,Re^{-0.08} \qquad (22)$$

Thus Fig. 15 includes four sets of data each of which necessarily cover a very narrow range of physical process parameters such as solution viscosity, density, diffusion coefficient etc., so

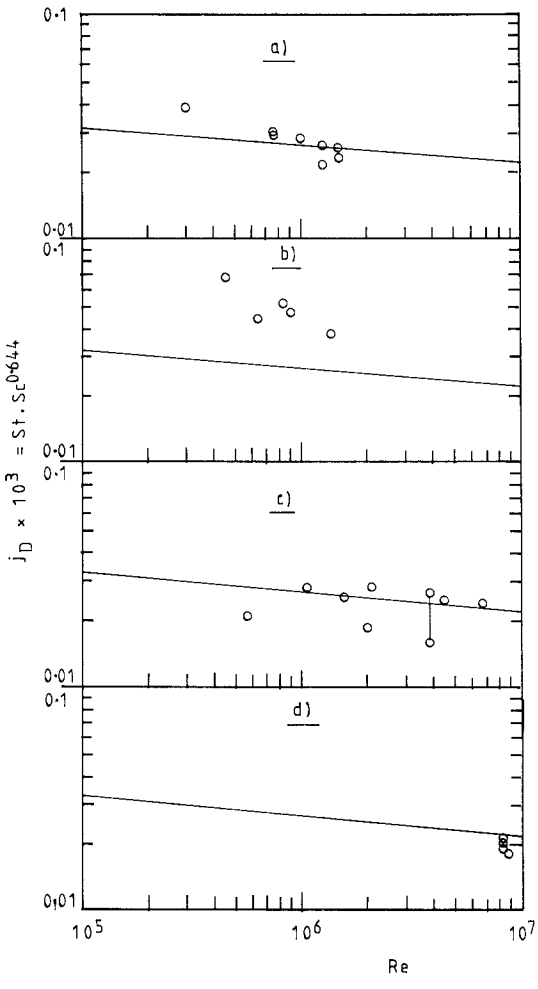

Fig. 15. Mass transfer for ECO-CELL plant. (a) 50 A laboratory rig, (b) 100 A mini-cell, (c) 500 A small pilot plant and, (d) 2000 A large pilot plant. Copper deposition from acid sulphate solution at 60°.C. Full lines represent the Holland equation for power depositions (Equation 22).

that any correlation must have a restricted degree of confidence. Yet, if a composite plot is made to compare the data with those correlations discussed in Parts I and II, self-consistency can be obtained. Such a composite plot is attempted in Fig. 16, which includes the correlation for a smooth cylinder after Eisenberg *et al.* [14, 15]:

$$j'_D = 0.079\, Re^{-0.3} \tag{23}$$

and the relationship for saturated roughness due to Theodorsen and Regier [16]:

$$j'_D = \left(1.25 + 5.76 \log_{10} \frac{d}{\varepsilon}\right)^{-2} \tag{24}$$

which is valid for

$$Re \geqslant \left(11.8 \frac{d}{\varepsilon}\right)^{1.18} \tag{25}$$

Three lines are shown in Fig. 16 corresponding to Equation 24, with d/ε values of 1000, 100 and 40. The degree of scale-up for the ECO-CELL data should be noted: the increase in cylinder diameter is up to six times while the consequent area increase is almost thirty times.

The expected degree of mass transport enhancement due to metal deposit roughness formation may be calculated for a range of hypothetical conditions relating to those used in service. Equation 16 may be rewritten in terms of the mass transport coefficient:

$$K_L = 0.0791\, U Re^b Sc^{-0.644} \tag{26}$$

K_L values may now be calculated for various

Table 5. Comparison of predicted mass transfer at smooth and rough (ECO-CELL) rotating cylinders

Rotational speed ω(revs min^{-1})	*Peripheral velocity* U(cm s^{-1})	*Mass transport coefficient,* K_L(cm s^{-1})		*Enhancement ratio* $=(B)/(A)$
		*Smooth cylinder (A)**	*ECO-CELL (B)†*	
19	10	0.00738	0.056	7.6
191	100	0.0370	0.466	12.6
1910	1000	0.185	3.873	20.9

$Sc = 1000$, $d = 10$ cm, $\nu = 0.01$ cm^2 s^{-1}.
*According to Equation 23.
†According to Equation 22.

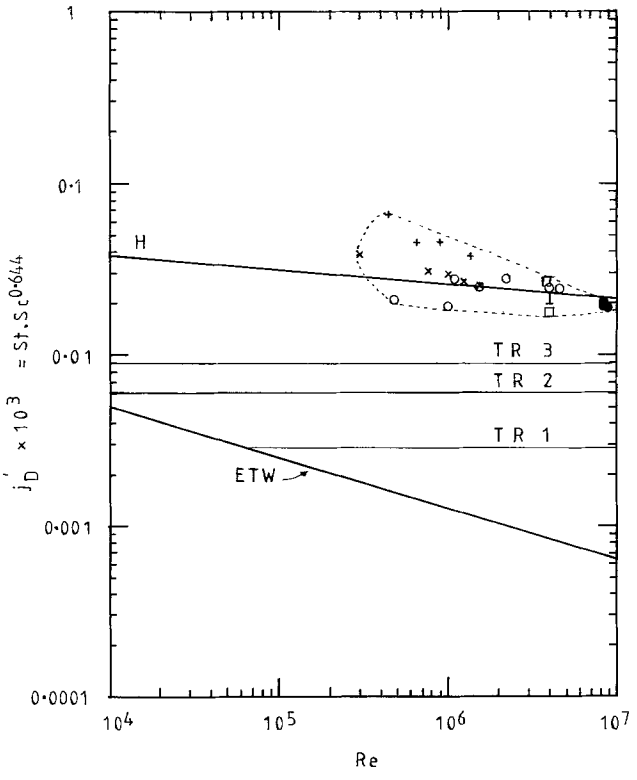

Fig. 16. Composite plot of mass transfer data with comparative literature correlations superimposed; data envelope referes to five separate reactors H: Equation 22, ETW: Equation 23, TR: Equation 24, TRI, d/ε = 1000, TR2, d/ε = 200; TR3, d/ε = 40. Data: × 50 A, laboratory rig, + 100 A, mini-cell, ○ 500 A, small pilot plant, ●2000 A, large pilot plant and ▣ 500 A, mobile rig.

rotation rates under hydrodynamically smooth ($b = 0.30$) and rough conditions due to metal powder deposition ($b = -0.08$) For the purpose of calculation, the following typical values have been taken:

$$Sc = 1000, \quad d = 10\,\text{cm}^2\text{s}^{-1} \quad \nu = 0.01\,\text{cm}^2\text{s}^{-1} \tag{26}$$

As Table 5 indicates, enhancement ratios from 8 to 21 are derived.

It is inevitable that in making a comparison between fundamental mass transfer studies and those obtained on pilot or production plants doubts regarding accuracy, precision etc., must exist. Particular limitations which ought to be recognized include:

(a) Limiting currents cannot be accurately defined and current efficiencies may fall below 90%.

(b) The rough powdered surface may be said to be saturated but not otherwise defined.

(c) Physical parameters of viscosity, density etc. were not measured each time.

(d) Comparatively few data points were obtained and only a few process variables were systematically varied.

(e) Reproducibility is rather poor in the large reactors in comparison to the more controlled laboratory cells; differences in design and construction exist between the various pilot plant reactors.

(f) In the large reactors much higher values of $Re(10^5 < Re < 10^7)$ are developed than is generally possible in the small laboratory cells. Nevertheless, the degree of mass transport rate enhancement is substantial rather than marginal and justifies the use of the empirical design Equation 3.

$$I_{Cu} = KCU^x \tag{27}$$

which may be written in the form of a dimensionless correlation

$$St\,Sc^{0.644} = 0.0791\,Re^p \tag{28}$$

where $p = -(1 - x)$ in power forming conditions for the narrow range of Re and Sc generally encountered. Values of p have been calculated from the whole range of fully documented data (see Table 6) and the design value

Table 6. Values of powder index 'p' obtained in various ECO-CELL plants

ECO-CELL plant (Nominal current)	*Temperature* (° C)	Peripheral velocity $U(cm\,s^{-1})$	*Powder* index* (p)
Laboratory rig (50A)	60	239–1200	−0.076
			−0.068
			−0.085
			−0.045
			−0.081
	60	400	−0.087
Mini-cell (100 A)	40	531	−0.046
	50	531	−0.032
	60	266	−0.012
	60	531	−0.038
	60	797	−0.052
Small pilot plant (500 A)	60	123–1698	−0.085
Mobile rig (500 A)	30	987	−0.080
	60	970	−0.07
	60	978	−0.07
	60	975	−0.09
	60	973	−0.10
	60	310	−0.07
Large pilot plant (2000A)	60	1086	−0.088
		1112	−0.080
			−0.082

*Defined by Equation 28.

of $p = -0.08 (x = +0.92)$ corresponding to Equation 16 is seen to be a conservative figure in terms of mass transfer enhancement.

The problem of obtaining mass transfer data for the cascade cells is much more difficult and has not yet been adequately solved. Ideally, individual cathode compartments should each operate at a potential corresponding to deposition at or near the limiting current to ensure maximum duty and current efficiency. Such operations may be monitored by potential profile measurements, the correct working potential being chosen with the aid of auxilliary polarization curves over the relevant range of concentration and taking due regard to the *IR* drops in the circuit. In practice, individual compartments may vary considerably in their behaviour if bypassing or leakage occurs at baffles and this has been discussed elsewhere [8]. For this reason it is more satisfactory to define performance as a fractional conversion averaged over the whole cascade assembly from which an average mass transfer coefficient may be calculated from the equation:

$$(f_R)_n = 1 - \frac{1}{(1 + K_L A/N)^n} \qquad (29)$$

Thus fractional conversions of 0.33 or 0.45 in each of the ten compartments are equivalent to K_L values of 0.38 or $0.53\,cm\,s^{-1}$ for a ten-compartment cascade reactor. A cascade of continuously stirred tank reactors is clearly a powerful assembly, capable of high overall conversions and, more particularly, very low exit metal concentrations while maintaining a high volumetric throughput. In comparison with other high conversion reactors it does not suffer from relatively high pressure drops as in packed bed or filter press cells and the product can be removed as a solid for reuse.

Acknowledgements

The authors acknowledge the help and assistance provided by staff at Ecological Engineering Limited (now part of Streetley Engineering Limited). Valuable advice, support and expertise was given by Dr F. S. Holland the inventor of the ECO-CELL process and Mr N. A. Gardner over a period of some years. Financial support from the Science Research Council (to FCW) is also acknowledged. Mr D. Robinson and Mr J. Mason provided technical assistance with pilot plant operation. Dr R. J. Marshall read the manuscript and made some helpful comments.

References

[1] D. R. Gabe and F. C. Walsh, *J. Appl. Electrochem.* **14** (5) (1984) 555.
[2] *Idem ibid.* **14** (5) (1984) 565.
[3] F. S. Holland, British Patent 1 505 736 (1978); US Patent. 42028 199 (1977).
[4] *Idem, Chem. Ind. (Lond)* (1978) 453.
[5] F. S. Holland and H. Rolskov, Effluent Water Treatment Convention, (Birmingham 1978).
[6] D. R. Gabe and F. C. Walsh, Proceedings Interfinish 80, Kyoto, Japan, (1980) p. 486.
[7] F. C. Walsh and D. R. Gabe, *Surface Technol.* **12** (1981) 25.
[8] F. C. Walsh, N. A. Gardner and D. R. Gabe, *J. Appl. Electrochem.* **12** (1982) 299.
[9] D. R. Gabe and F. C. Walsh, in 'Electroplating Engineering and Waste Recycling: New Developments and Trends' (edited by D. D. Snyder,

U. Landau and R. Sard), Electrochemical Society, Pennington, NJ (1983) pp. 367–383.
[10] F. S. Holland and F. C. Walsh, British Patent Appl. 81-04624 (1982).
[11] F. C. Walsh and D. R. Gabe, *J. Appl. Electrochem.* **11** (1981) 117.
[12] N. A. Gardner and F. C. Walsh, in 'Electrochemical Cell Design' (edited by R. E. White), Plenum Press, New York (1984) pp. 225–258.
[13] A. T. S. Walker and A. A. Wragg, *Electrochimica Acta.* **22** (1977) 1129.
[14] M. Eisenberg, C. W. Tobias and C. R. Wilke, *Chem. Eng. Progr. Symp. Ser.* **51** (1955) 1.
[15] *Idem, J. Electrochem. Soc.* **101** (1954) 306.
[16] T. Theodorsen and A. Regier, Nat. Advisory Committee Aeronautics Report No. 793 (1944).